Supporting Information for the *Environmental Science and Technology* article:

Oxidation of Antibacterial Compounds by Ozone and Hydroxyl Radical: Elimination of Biological Activity during Aqueous Ozonation Processes

Michael C. Dodd,[†,‡] Hans-Peter E. Kohler,[†] Urs von Gunten,[†,‡,*]

[†] Eawag: Swiss Federal Institute of Aquatic Science and Technology, 8600 Duebendorf, Switzerland

[‡] Institute for Biogeochemistry and Pollutant Dynamics, ETH Zurich, 8092 Zurich, Switzerland

*Corresponding author phone: +41 44 823 52 70; fax: +41 44 823 52 10

Author e-mail addresses: michael.dodd@eawag.ch, hkohler@eawag.ch, vongunten@eawag.ch

23 pages, including 4 narratives, 1 table, and 13 figures

Text S1. Oxidation of antibacterial model compounds.

Ozone. Solutions of each of the antibacterial compounds listed in Table S1 (aside from triclosan (TRI), for which O_3 data were previously obtained as described in (*1*)) were prepared in 1-mM, pH 7 phosphate buffer at initial concentrations of 10 μM, with the exceptions of sulfamethoxazole (SMX), azithromycin (AZ), and lincomycin (LM), which were prepared at 50, 50, and 200 μM, respectively. These solutions were dosed with 5 mM of *t*-BuOH (used as a $^{\bullet}OH$ scavenger) and distributed in 20-mL volumes amongst eleven 30-mL, amber, borosilicate glass vials (Scheme 1 in the main text). The vials were then placed in a 20 (±0.5) °C water bath placed on top of a 15-position magnetic stir plate. After thermal equilibration, and under constant, rapid stirring, 10 of the vials were dosed with O_3 over a range of concentrations sufficient to cover from between approximately 0.1- to 2-log depletion of the respective parent compound, by directly injecting various volumes of ~1.3-1.5-mM O_3 stock via gas-tight, glass syringe. The eleventh vial was left untreated, as a negative O_3 control. All vials were then capped and allowed to sit for at least 12 hrs prior to sampling to ensure complete decomposition of O_3 residual in the treated solutions. Four-mL samples of each catalase-treated solution were then transferred to 4-mL amber, borosilicate glass, screw-top vials (or polystyrene culture tubes in the case of CF and EF), treated with ~64 units/mL of thymol-free catalase, and allowed to react for at least 1 hour at ambient temperature (20-25 °C) to quench H_2O_2 produced during O_3 treatment. These samples were then capped and stored at 4 °C until analysis of residual parent antibacterial compounds (by HPLC-UV, according to (*2*)) and assay of residual antibacterial activity (according to the microdilution method described below) during the following week. Samples containing less stable antibacterial model compounds (e.g., PG and CP) were analyzed no later than three days after preparation. Amikacin (AM) was derivatized with 9-fluoroenylmethyl chloroformate (FMOC) (*3*) immediately prior to HPLC analysis, to permit UV detection.

Hydroxyl radical (˙OH). For the majority of compounds investigated, ˙OH was generated in situ by γ-radiolysis (via a lead-shielded ^{60}Co source) of aqueous solutions, according to (*4*). Briefly, 100-mL solutions of each model compound were prepared in 1-mM, pH 7 phosphate buffer at initial concentrations of 10 μM for tylosin (TYL), ciprofloxacin (CF), enrofloxacin (EF), trimethoprim (TMP), tetracycline (TET), vancomycin (VM), and AM, 50 μM for SMX and AZ, or 5 μM for TRI, then dosed to borosilicate glass reactors (Scheme 1), and purged with a 4:1 mixture of N_2O:O_2. Prior to irradiation, a 1.5-mL sample was taken from each solution as a control. Each solution was then irradiated for repeated pre-defined time intervals up to ten total irradiation periods sufficient to achieve ~90% or greater depletion of the parent compound. After each irradiation interval, 1.5-mL samples were withdrawn from these solutions, transferred to amber, borosilicate, screw-top autosampler vials (or polystyrene culture tubes in the case of CF and EF), and capped for storage at 4 °C. All samples were subsequently subjected to HPLC analysis (according to (*2*)) and microbiological activity assay (as described below) within the following week. AM was derivatized prior to HPLC analysis, as described above. As in the case of O_3-treated solutions, all γ-irradiated solutions were treated with thymol-free catalase (~106 units/mL) and allowed to react at ambient temperature (20-25 °C) for at least 1 hour prior to microbiological assay.

Cephalexin (CP) was treated with ˙OH generated via UV-photolysis of H_2O_2 using a 500-W medium pressure Hg lamp with emission wavelengths < 308 nm screened by a UV-cutoff filter to minimize direct CP photolysis. One-mM, pH 7 phosphate solutions were dosed with 10 μM of CP and 10 mM of H_2O_2, sampled to obtain an untreated control, and then irradiated in 30-mL quartz test tubes (Scheme 1) for pre-defined time intervals up to total irradiation periods sufficient to achieve at least 90% depletion of the parent compound. Following each irradiation period, 1.5-mL samples were withdrawn from these solutions and immediately transferred to amber, borosilicate glass, screw-top autosampler vials containing

15 μL of 6380 unit/mL thymol-free catalase. After at least 1 hour at ambient temperature (20-25 °C), samples were then either prepared for residual substrate analysis and microbiological assay, or placed under storage at 4 °C until HPLC analysis and microbiological assay within the following 1-2 days. Experiments included a minimum of 10 different irradiation times. Direct photolytic losses of CP were demonstrated via negative H_2O_2 control to be no more than ~1.2% during the full irradiation period.

Roxithromycin (RX), penicillin G (PG), and lincomycin (LM) samples were prepared and analyzed in the same manner as those for CP, except that $^{\bullet}OH$ was generated via UV-photolysis of H_2O_2 using a 15-W low pressure Hg lamp ($\lambda_{max,emission}$ ~ 254 nm) without a cutoff filter. Solutions were prepared at initial model compound concentrations of 10 μM for RX and PG, and 200 μM for LM, and dosed with an initial H_2O_2 concentration of 5-10 mM. Direct photolytic losses of PG were demonstrated via negative H_2O_2 control to be no greater than ~1.4% during the full irradiation period, whereas RX and LM are each transparent at the UV wavelengths utilized for these experiments.

Text S2. Measurement of antibacterial activities after treatment with O_3 and $^{\bullet}OH$.

Broth microdilution assay. With the exception of $^{\bullet}OH$-treated triclosan solutions, the activities of antibacterial solutions prepared according to the procedures described above were quantified in triplicate by means of a microdilution assay based on the NCCLS clinical microdilution standard (*5*) (Scheme 1). Prior to biological assay, all oxidized solutions were allowed to sit for at least 1 hour following treatment with ~64 units/mL of thymol-free catalase to quench any residuals of H_2O_2 generated in situ or remaining from H_2O_2 photolysis experiments. Ten-member dilution series were then prepared from each sample via 1:1 serial dilution of the sample in 1-mM phosphate buffer (also containing 5-mM of *t*-BuOH in the case of O_3-treated samples), across an individual row of the corresponding 96-well microtiter

plate. Prior to preparation of serial dilution series, all PG samples were pre-diluted by a factor of 2, all CF samples by a factor of 10, O_3-treated EF samples by a factor of 5, $^{\bullet}OH$-treated EF samples by a factor of 10, and all AZ samples by a factor of 5 in 1-mM, pH 7 phosphate buffer (also containing 5-mM of *t*-BuOH for O_3-treated samples), due to the high potencies of each of these compounds at the initial concentrations used in each oxidation experiment. Matching standard dilution series were prepared from the untreated samples of each parent antibacterial compound for assay with the oxidant-treated samples. Each sample and standard solution volume was then inoculated with an equal volume of Mueller-Hinton broth containing 1 x 10^6 CFU/mL of the reference *E. coli* or *B. subtilis* strains, sealed with either paraffin or breathable Rayon sealing tape to minimize evaporative water loss, and incubated with 200 rpm agitation, at 37 °C (for *E. coli* cultures) or 30°C (for *B. subtilis* cultures), for 8 h. After incubation, the paraffin or sealing tape was removed, the plates were re-sealed with impermeable polyester sealing tape, and each plate was agitated vigorously using a Vortex microtiter plate shaker to re-suspend any pelleted cell material from the bottoms of the microtiter wells. Subsequently, the polyester tape was removed and absorbances of the solutions in each microtiter well were measured at 625 nm (as a surrogate for cell density (*5*)), using a Spectra Rainbow microplate reader (Tecan, Switzerland).

Analysis of microdilution dose-response data. The relationships between sample dilution and corresponding growth inhibitions, *I* (in %), for the respective reference inocula were then quantitatively evaluated for all antibacterials other than CF, EF, and AM, and TRI by simultaneous non-linear regression of the 11 replicate data-sets corresponding to the untreated standard and 10 samples collected for treatment by each oxidant, via eq S1,

$$I(\%) = I_{\min} + \frac{I_{\max} - I_{\min}}{1 + 10^{\left(\log\left(\mathrm{EC}_{50}/\left(1/m^n\right)\right)\times \mathrm{H}\right)}} = I_{\min} + \frac{I_{\max} - I_{\min}}{1 + \left(\mathrm{EC}_{50}/\left(1/m^n\right)\right)^{\mathrm{H}}} \quad \text{(S1)}$$

using GraphPad Prism (GraphPad Software), where EC_{50} represents the effective antibacterial concentration (or in this case, sample dilution) at which 50% growth inhibition is observed, *m*

represents the dilution factor for each serial dilution step (i.e., 2 in this case), *n* is the number of times a given member of the dilution series has been diluted relative to the parent sample, H represents the Hill slope inherent to the dose-response relationships for each combination of antibacterial compound and reference bacterial strain, and I_{max} and I_{min} represent the maximum and minimum growth inhibition values for a given data set, respectively. To maximize regression accuracy, Prism was constrained to solve simultaneously for the shared, best-fit values of H, $I_{max,t}$, and $I_{min,t}$ characterizing dose-responses for all replicates of each 11-member sample set, while $\log EC_{50}$ was allowed to vary.

Dose-response relationships for CF, EF, and AM were evaluated by fitting sample data to the five-parameter modified Hill model (i.e., the Richard's equation (*6*)) represented by eq S2 (also using GraphPad Prism),

$$I(\%) = I_{min} + \frac{I_{max} - I_{min}}{\left(1 + 10^{\left(\log EC_{50} - \log\left(1/m^n\right)\right)\times H}\right)^S} = I_{min} + \frac{I_{max} - I_{min}}{\left(1 + \left(EC_{50}/\left(1/m^n\right)\right)^H\right)^S} \quad \text{(S2)}$$

where EC_{50}, *m*, *n*, H, I_{max}, and I_{min} are the same as in eq S1, and S is a parameter quantifying the asymmetry of a given dose-response curve's slope.

Uncertainties (as 95% confidence limits) for each of the microdilution measurements described here were determined according to Supporting Information, Text S3.

Broth macrodilution assay. The macrodilution methodology utilized for measurement of residual activity in •OH-treated solutions of triclosan (TRI) was essentially the same as that described in (*1*), with several minor exceptions. Briefly, 120-μL aliquots of •OH-treated TRI solutions ($[TRI]_0$ = 5 μM) – prepared as described above – were added to glass culture tubes containing 1.38 mL of 1-mM, pH 7 phosphate buffer (to yield 12.5-fold dilution of the original samples). In addition, 360 μL of the untreated 5-μM TRI solution was dosed to a glass culture tube containing 4.14 mL of 1-mM phosphate buffer (to yield 12.5-fold dilution of the original sample). A set of eleven 2:1 serially-diluted standards was then prepared by transferring 3 mL of the 12.5×-diluted TRI standard to a culture tube containing 1.5 mL of 1-

mM, pH 7 phosphate buffer, mixing, then transferring 3-mL of the resulting solution to another 1.5-mL buffer volume, and so on, to yield a series of TRI standards with [TRI] ranging from 4.0 x 10^{-7} M to 6.9 x 10^{-9} M. Each of the culture tubes contained within the 11-member sample and standard sets was subsequently inoculated with 1.5 mL of a broth *E. coli* K12 culture containing approximately 1 x 10^{6} CFU/mL, capped, incubated at 37° C under constant agitation (200 rpm on a rotating shaker plate), and processed for analysis as described previously (*1*). As before, absorbance measurements were obtained for each sample at 625 nm after appropriate incubation periods.

Analysis of macrodilution dose-response data. Dose-response relationships were obtained for serially-diluted TRI standards by plotting inhibition vs. the in vitro assay concentration of triclosan and fitting the data to eq S3 (using GraphPad Prism),

$$I(\%) = I_{\min} + \frac{I_{\max} - I_{\min}}{1 + 10^{\left(\log\left(EC_{50}/[TRI]_{\text{in vitro}}\right) \times H\right)}} = I_{\min} + \frac{I_{\max} - I_{\min}}{1 + \left(EC_{50}/[TRI]_{\text{in vitro}}\right)^{H}} \quad \text{(S3)}$$

where $[TRI]_{\text{in vitro}}$ is the in vitro concentration of TRI present in a given culture tube after any preceding dilution steps, and all other variables are as in eq S1. The $I_{\min}$, $I_{\max}$, EC_{50}, and H terms obtained by fitting eq S3 to the standard data set were then used to calculate theoretical *I* values for the residual $[TRI]_{\text{in vitro}}$ values present in each oxidant-treated TRI sample for comparison with the corresponding measured *I* values. All sample and standard activity assays processed by this method were performed in triplicate. Uncertainties (as 95% confidence limits) were calculated for all macrodilution measurements according to Text S3.

Text S3. Error calculations for microdilution and macrodilution assay data

Microdilution assay error calculations. Standard errors of the calibration curves used in HPLC analyses of each model compound were multiplied by the appropriate t-distribution constants to obtain 95% confidence intervals of individual concentration measurements, [C]. Overall confidence intervals for each $[C]/[C]_0$ value were then calculated by propagating the

confidence limits of each [C] measurement through the error function obtained via partial differentiation of the expression, $[C]/[C]_0$, with respect to [C] and $[C]_0$. Ninety-five percent confidence intervals were calculated for each EC_{50} value by first multiplying the anti-log of the logarithmic standard errors generated by Prism for each $\log EC_{50}$ value by a t-distribution constant of 1.967 or 1.968, calculated from: (a) d.f. = 3 replicates x 11 samples x 10 serial dilutions/sample - 14 variables = 316, or (b) d.f. = 3 replicates x 11 samples x 10 serial dilutions/sample - 15 variables = 315, where the variables here are the 11 sample-specific values of EC_{50} and either (a) the 3 shared values of H, $I_{max,t}$, and $I_{min,t}$ for eq S1, or (b) the 4 shared values of H, $I_{max,t}$, $I_{min,t}$, and S for eq S2) to obtain linearized error coefficients. The resulting linearized error coefficients were next multiplied or divided by the appropriate EC_{50} values to obtain the corresponding positive or negative confidence interval, respectively, for each individual EC_{50} value. Ninety-five percent confidence intervals were then calculated for each PEQ ($= EC_{50,0}/EC_{50}$) value in the same manner as for $[C]/[C]_0$.

Macrodiluation assay error calculations. Ninety-five percent confidence intervals for each $[TRI]_{in\ vitro}$ value were calculated according to the same procedure used for concentration measurements obtained in the microdilution assays described above. However, as no serial dilutions of TRI samples other than the control were performed (precluding measurement of EC_{50} values for all but the control), uncertainties in *E. coli* K12 responses to the oxidant-treated samples were instead calculated for individual *I* measurements as follows. First, 95% confidence intervals of triplicate *I* values were calculated from the standard deviations of raw absorbance measurements, A, for each sample replicate and for the respective A_{min} and A_{max} values obtained from replicate negative and positive growth controls. The resulting confidence interval calculations were then propagated through the error function obtained via partial differentiation of eq 1 in the main text with respect to A, A_{min}, and A_{max} to obtain overall 95% confidence limits for each *I* value.

Likewise, uncertainties of the theoretical I values predicted for the $[TRI]_{in\ vitro}$ values of each oxidant-treated TRI sample (using the fitted model parameters obtained from the control data set) were determined by propagating the 95% confidence limits corresponding to the I_{min}, I_{max}, EC_{50}, and H values obtained via GraphPad Prism for the untreated TRI control data set, in addition to those for the measured $[TRI]_{in\ vitro}$ values of each oxidant-treated sample (calculated as described above), through the error function obtained via partial differentiation of eq S3 with respect to each of these variables.

Random or unquantified error in microdilution and macrodilution assays. Although every effort was undertaken to control for possible sources of error, random (as opposed to systematic) positive or negative deviations from the ideal case beyond calculated uncertainty limits were still observed in some measurements; most likely as a consequence of unquantified, non-systematic methodological uncertainties associated with such factors as evaporative water loss in the microdilution assay or variable derivatization yields in the case of amikacin (AM) analyses.

Text S4. Correlations amongst observed O_3 target sites for antibacterial model compounds, their roles in mediating target-specific antibacterial activities, and measured stoichiometries of antibacterial model compound deactivation by treatment with O_3

Macrolides. Measured antibacterial activities of the three macrolide antibacterial compounds, RX, AZ, and TYL, following treatment with O_3, are depicted in Figure 2a in the main text. As shown here, RX exhibits an apparent deactivation stoichiometry of approximately one PEQ lost per mole fraction equivalent of RX consumed by direct reaction with O_3. This value is consistent with findings previously reported for deactivation of the structurally-analogous macrolide clarithromycin by O_3 (*7*), and agrees with the mechanism by which macrolide antibacterials are believed to derive their biochemical activity; that is, from specific hydrogen bonding with various nucleobases and phosphodiester linkages in the

peptidyl transferase cavity of bacterial 23S rRNA (*8*). The bonding interaction most likely to be interrupted by direct reaction with O_3 is that involving RX's tertiary amine (Table S1), which is the primary site of attack by O_3 (*2, 7, 9*). Modification of the tertiary amine via oxidation to the corresponding *N*-oxide or via demethylation (*7, 10*) should prevent its hydrogen bonding with 23S rRNA, leading to reduction or elimination of each parent macrolide's antibacterial activity. As shown in Figure 2a, AZ (a fifteen-membered macrolide) and TYL (a sixteen-membered macrolide) are also deactivated with apparently ideal stoichiometry upon reaction with O_3, in agreement with the previously reported observation that their tertiary desosamine moieties (Table S1) are also the primary sites of attack by O_3 at circumneutral pH (*2*). As nearly all macrolides contain the characteristic desosamine sugar moiety, these findings can presumably be generalized across most of the macrolide antibacterial structural class; permitting one to conclude that O_3 can effectively deactivate not only macrolides possessing the 14-member macrolactone ring template, but also those possessing 15- and 16-membered rings.

Fluoroquinolones. According to the data presented in Figure 2b in the main text, CF and EF - which are differentiated only by the degree of their N4 atoms' alkyl substitution (Table S1), each exhibit stoichiometric deactivation upon direct reaction with O_3. Fluoroquinolones derive their biochemical activity from blockage of DNA replication, via several highly specific hydrogen-bonding and charge interactions with relaxed bacterial DNA in the presence of DNA topoisomerase enzymes (*8, 11*). According to a widely accepted model for fluoroquinolone-DNA binding (*11*), the characteristic quinolone moiety is responsible for these interactions. Consequently, one would expect that oxidation of this moiety by O_3 would generally be required to achieve substantial reduction or elimination of fluoroquinolones' antibacterial potencies. However, the heterocyclic N4 amines of the piperazine moieties present in the CF and EF parent molecules (Table S1) represent the primary sites at which CF and EF react with O_3, whereas reactions at the model compounds'

quinolone moieties are actually quite slow (*2*). Thus, even modification of the N4 amine (via oxidation to the corresponding *N*-oxide or partial dealkylation (*7*, *10*)) appears to modify the fluoroquinolone structures to a degree sufficient to diminish either fluoroquinolone access to the bacterial cell target or the binding interactions necessary for their interruption of DNA replication once inside the cell. These observations are expected to be broadly applicable amongst members of the fluoroquinolone structural class containing the piperazine moiety.

Sulfonamides. Deactivation stoichiometries for SMX are depicted in Figure 2d in the main text. As illustrated by these data, SMX also exhibits stoichiometric deactivation upon reaction with O_3. This is consistent with prior identification of the *p*-sulfonylaniline moiety (Table S1) as the primary site at which the SMX molecule is attacked by O_3 (*2*), as this characteristic moiety is directly responsible for every sulfonamide antibacterial compound's interference with bacterial folate synthesis (*8*). Namely, modification of this moiety - via oxidation of the aromatic amine (*12*), or by ring opening pathways characteristic of reactions between O_3 and activated aromatics (*13*) - would be expected to preclude SMX's function as a competitive analogue of *p*ABA (*8*). Although certain sulfonamides possess alternative heterocyclic substituents (in place of the dimethylisoxazole moiety shown for SMX - Table S1) that may also be rapidly oxidized by O_3, reactivity of the *p*-sulfonylaniline moiety should generally be sufficiently high (*2*, *9*) to ensure that all sulfonamide antibacterial agents will be efficiently deactivated by direct reaction with O_3.

Dihydrofolate Reductase (DHFR) Inhibitor. As shown in Figure 2d, TMP is also stoichiometrically deactivated upon reaction with O_3. This is consistent with identification of the 2,4-diaminopyrimidine structure (Table S1) as the primary target of direct attack by O_3 at circumneutral pH (*2*), as the intact 2,4-diaminopyrimidinyl structure plays a critical role in enabling TMP's ability to inhibit bacterial folate synthesis (*8*). That is, modification of this moiety - via oxidation of an aromatic amine (*12*), or by the ring opening/contraction pathways characteristic of reactions between O_3 and the pyrimidine nucleobases (*14*, *15*) - would be

expected to eliminate TMP's ability to compete with the structural analogue 7,8-dihydrofolate for available DHFR by disrupting the specific modes of binding between the N1, 2-amino, and 4-amino nitrogens of the 2,4-diaminopyrimidine ring and target sites within the bacterial DHFR enzyme structure (*16*).

Lincosamide. The deactivation data shown in Figure 2d illustrate that direct reaction with O_3 also yields stoichiometric elimination of LM's biological activity. Previous kinetics measurements indicate that the initial reaction of O_3 with LM takes place at its tertiary pyrrolidine nitrogen (Table S1) at circumneutral pH, whereas secondary attack likely occurs at the LM thioether (*17*). Oxidation of the former by O_3 should proceed via *N*-oxide formation or dealkylation (*7*, *10*), whereas oxidation of the latter should lead to LM-sulfoxide (*18, 19*), which is known to possess significantly lower antibacterial potency than the parent structure (*20*). However, in neither case do these reactions occur at sites responsible for the specific hydrogen-bonding interactions between lincosamides and target nucleotides in bacterial 23S rRNA (*21*) that actually lead to inhibition of bacterial protein synthesis. These observations suggest that minor structural changes - even at spatially and electronically isolated regions of the LM structure - are sufficient to either hinder LM access to bacterial target sites or to disrupt the H-bonding patterns ultimately responsible for LM's and other lincosamides' antibacterial activities. Analogous reaction mechanisms and outcomes are expected to apply to the clinical-use lincosamide, clindamycin, on account of its nearly identical structure.

Tetracycline. The data shown in Figure 2d illustrate that oxidation of TET by O_3 results in rapid, stoichiometric elimination of the former's antibacterial activity. This is consistent with evidence that reactions of O_3 with TET proceed by attack of the latter's fused tetracyclic system at circumneutral pH (*2*). As the tetracycline structure is likely extensively modified upon direct reaction with O_3 via O-addition to or ozonolysis of its aromatic and olefinic structural moieties (*13, 22*), the requisite charge interactions (direct and/or metal-mediated) of the tetracycline molecule's keto and hydroxy oxygens (Table S1) with specific

internucleotide phosphodiester linkages of the bacterial ribosome would likely be disrupted (*8*), leading to loss of the antibacterial molecule's biological activity. These observations can likewise be expected to apply to nearly all tetracycline antibacterials, due to conservation of the fundamental tetracycline system throughout the structural class (*23*).

Glycopeptide. The data shown in Figure 2d indicate that the reaction of O_3 with VM also yields an apparent loss of one PEQ per fractional mole equivalent of VM consumed. These data indicate that chemical modifications by O_3 disrupt the glycopeptide structure's interactions with cellular targets to a degree sufficient to substantially diminish VM's antibacterial potency. More specifically, although the hydroxyphenol, trimethylbenzyl, and *N*-methylleucine moieties identified as the most probable sites at which VM is attacked O_3 at circumneutral pH (*2*) are not directly involved in the hydrogen-bonding interactions responsible for bacterial peptidoglycan sequestration (the explicit means by which glyocopeptides inhibit cell wall synthesis (*8*)), their oxidation by O_3 should lead to disruption of the VM stereochemistry necessary for such specific H-bonding to occur (*13, 24*). This should in turn result in elimination of VM's antibacterial activity, as observed in Figure 2d.

Aminoglycoside. Although the data shown in Figure 2d for the AM-O_3 reaction deviate substantially from the plot of ideally stoichiometric deactivation at low AM turnovers, it is nevertheless clear from these and the data shown for higher O_3 doses that AM is efficiently deactivated by direct reaction with O_3. This finding is consistent with identification of AM's primary amines as the main sites of attack by O_3 at circumneutral pH (*2*), as these functional groups are believed to play an important role in both of the modes from which the aminoglycosides' antibacterial activities are derived; namely, bacterial rRNA hydrogen bonding and charge-interactions, and competitive displacement of the divalent cations, Mg^{2+} and Ca^{2+}, from the bacterial cell wall (*8*, *25*).

Table S1. Model antibacterial compounds (shown with $k_{O3,app}$" [a], primary O_3 targets [b], $k_{\bullet OH,app}$" [a] (all at pH 7), and applied bioassays

Roxithromycin (RX)

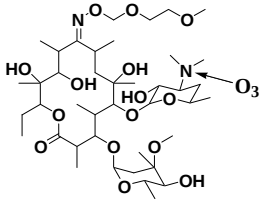

Assay: Microdil.
Bacterium: *B. subtilis*

$k_{O3,app,RX}$" = 6.3 x 10^4 $M^{-1}s^{-1}$
$k_{\bullet OH,app,RX}$" = 5.4 x 10^9 $M^{-1}s^{-1}$

Azithromycin (AZ)

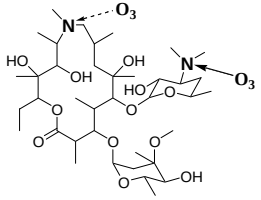

Assay: Microdil.
Bacterium: *B. subtilis*

$k_{O3,app,AZ}$" = 1.1 x 10^5 $M^{-1}s^{-1}$
$k_{\bullet OH,app,AZ}$" = 2.9 x 10^9 $M^{-1}s^{-1}$

Tylosin (TYL)

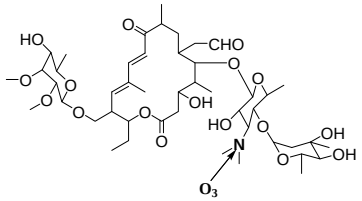

Assay: Microdil.
Bacterium: *B. subtilis*

$k_{O3,app,TYL}$" = 5.1 x 10^5 $M^{-1}s^{-1}$
$k_{\bullet OH,app,TYL}$" = 8.2 x 10^9 $M^{-1}s^{-1}$

Vancomycin (VM)

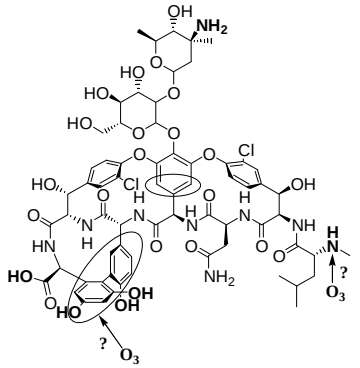

Assay: Microdilution
Bacterium: *B. subtilis*

$k_{O3,app,VM}$" = 6.1 x 10^5 $M^{-1}s^{-1}$
$k_{\bullet OH,app,VM}$" = 8.1 x 10^9 $M^{-1}s^{-1}$

Sulfamethoxazole (SMX)

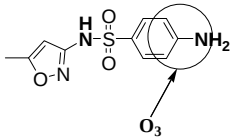

Assay: Microdil.
Bacterium: *E. coli*

$k_{O3,app,SMX}$" = 5.5 x 10^5 $M^{-1}s^{-1}$
$k_{\bullet OH,app,SMX}$" = 5.5 x 10^9 $M^{-1}s^{-1}$

Ciprofloxacin (CF)

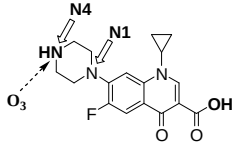

Assay: Microdil.
Bacterium: *E. coli*

$k_{O3,app,CF}$" = 1.9 x 10^4 $M^{-1}s^{-1}$
$k_{\bullet OH,app,CF}$" = 4.1 x 10^9 $M^{-1}s^{-1}$

Enrofloxacin (EF)

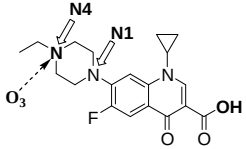

Assay: Microdil.
Bacterium: *E. coli*

$k_{O3,app,EF}$" = 1.5 x 10^5 $M^{-1}s^{-1}$
$k_{\bullet OH,app,EF}$" = 4.5 x 10^9 $M^{-1}s^{-1}$

Trimethoprim (TMP)

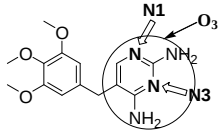

Assay: Microdil.
Bacterium: *E. coli*

$k_{O3,app,TMP}$" = 2.7 x 10^5 $M^{-1}s^{-1}$
$k_{\bullet OH,app,TMP}$" = 6.9 x 10^9 $M^{-1}s^{-1}$

Penicillin G (PG)

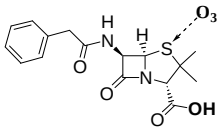

Assay: Microdil.
Bacterium: *B. subtilis*

$k_{O3,app,PG}$" = 4.8 x 10^3 $M^{-1}s^{-1}$
$k_{\bullet OH,app,PG}$" = 7.3 x 10^9 $M^{-1}s^{-1}$

Cephalexin (CP)

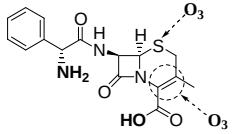

Assay: Microdil.
Bacterium: *B. subtilis*

$k_{O3,app,CP}$" = 8.7 x 10^4 $M^{-1}s^{-1}$
$k_{\bullet OH,app,CP}$" = 8.5 x 10^9 $M^{-1}s^{-1}$

Triclosan (TRI)

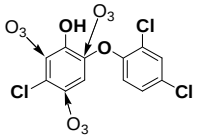

Assay: Macrodilution
Bacterium: *E. coli*

$k_{O3,app,TRI}$" = 3.8 x 10^7 $M^{-1}s^{-1}$
$k_{\bullet OH,app,TRI}$" = 5.4 x 10^9 $M^{-1}s^{-1}$

Lincomycin (LM)

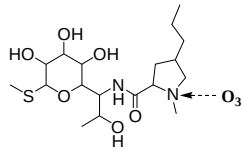

Assay: Microdil.
Bacterium: *B. subtilis*

$k_{O3,app,LM}$" = 6.7 x 10^5 $M^{-1}s^{-1}$
$k_{\bullet OH,app,LM}$" = 8.5 x 10^9 $M^{-1}s^{-1}$

Tetracycline (TET)

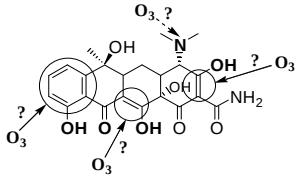

Assay: Microdil.
Bacterium: *E. coli*

$k_{O3,app,TET}$" = 1.9 x 10^6 $M^{-1}s^{-1}$
$k_{\bullet OH,app,TET}$" = 7.7 x 10^9 $M^{-1}s^{-1}$

Amikacin (AM)

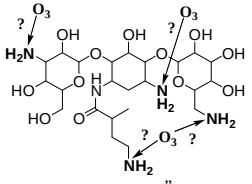

Assay: Microdil.
Bacterium: *E. coli*

$k_{O3,app,AM}$" = 1.8 x 10^3 $M^{-1}s^{-1}$
$k_{\bullet OH,app,AM}$" = 7.2 x 10^9 $M^{-1}s^{-1}$

[a] k_{app}" at pH 7 from (*2*, *9*, *17*)
[b] O_3 targets at pH 7 shown according to (*2*, *26*). Targets responsible for model compounds' antibacterial activities indicated by solid arrows; targets not responsible for activities indicated by dotted arrows.

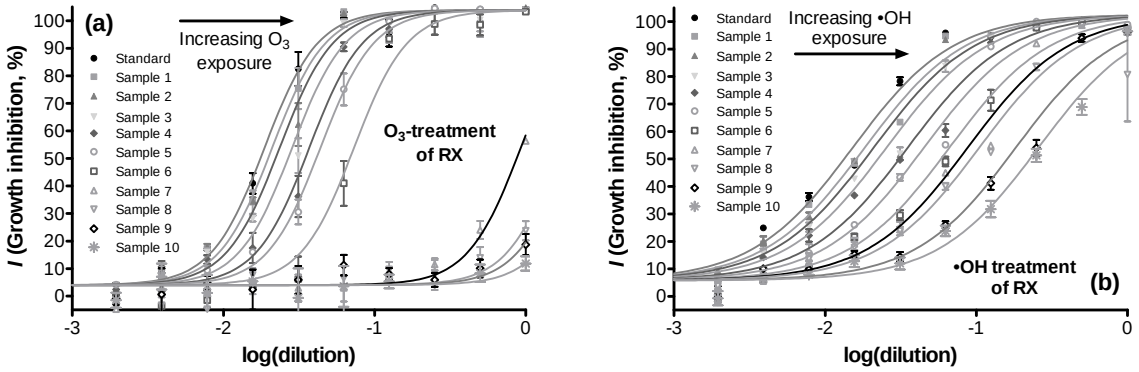

330

331 **Figure S1.** Dose-response relationships for oxidation of RX by (a) O_3 and (b) •OH.
332 Measurements of *I* (symbols) are depicted with 95% confidence intervals determined for
333 triplicate data sets, according to Text S3. Fits (lines) obtained using eq S1. The independent
334 variable "dilution" is determined as described in the caption to Figure 1 in the main text.

335

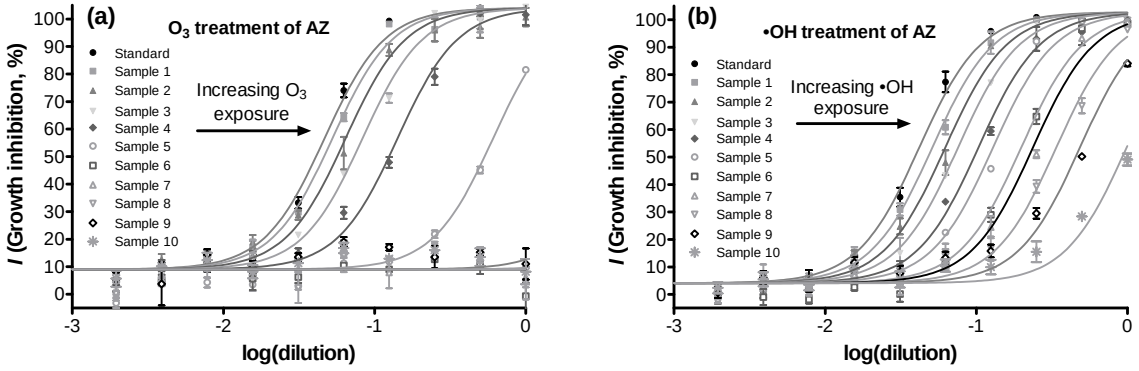

336

337 **Figure S2**. Dose-response relationships for oxidation of AZ by (a) O_3 and (b) •OH.
338 Measurements of *I* (symbols) are depicted with 95% confidence intervals determined for
339 triplicate data sets, according to Text S3. Fits (lines) obtained using eq S1. The independent
340 variable "dilution" is determined as described in the caption to Figure 1 in the main text.

341

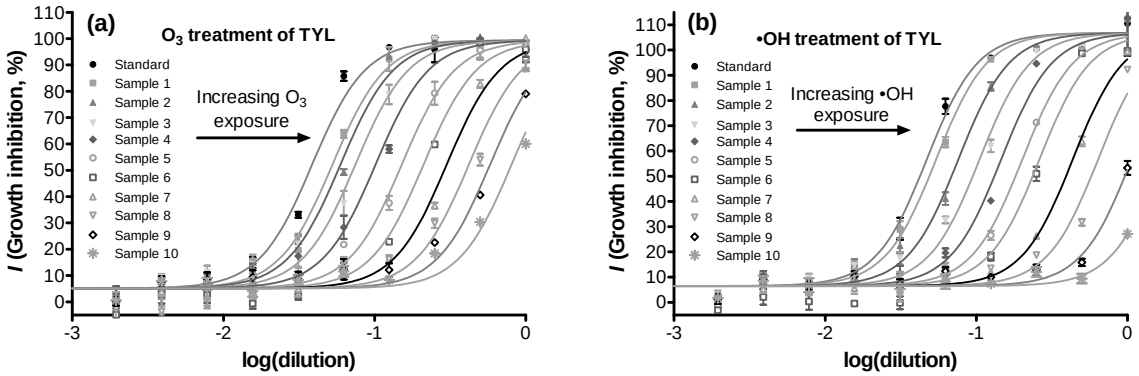

342

343 **Figure S3**. Dose-response relationships for oxidation of TYL by (a) O_3 and (b) •OH.
344 Measurements of *I* (symbols) are depicted with 95% confidence intervals determined for
345 triplicate data sets, according to Text S3. Fits (lines) obtained using eq S1. The independent
346 variable "dilution" is determined as described in the caption to Figure 1 in the main text.

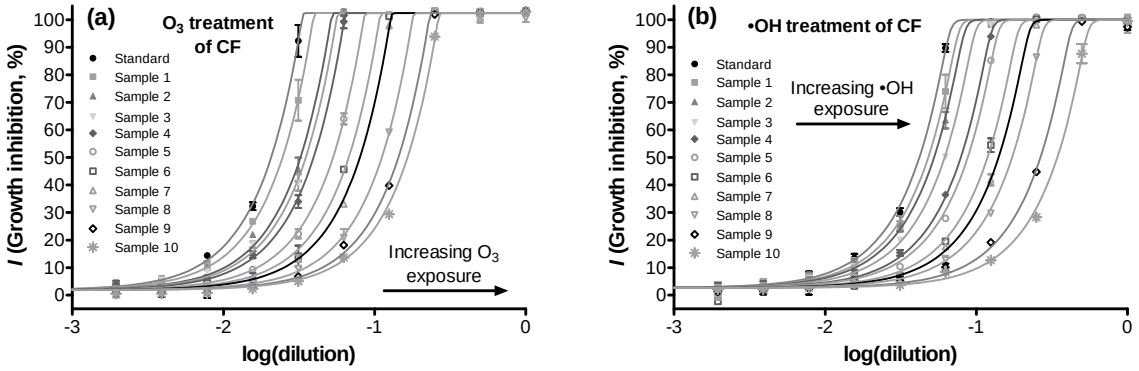

Figure S4. Dose-response relationships for oxidation of CF by (a) O_3 and (b) •OH. Measurements of *I* (symbols) are depicted with 95% confidence intervals determined for triplicate data sets, according to Text S3. Fits (lines) obtained using eq S2. The independent variable "dilution" is determined as described in the caption to Figure 1 in the main text.

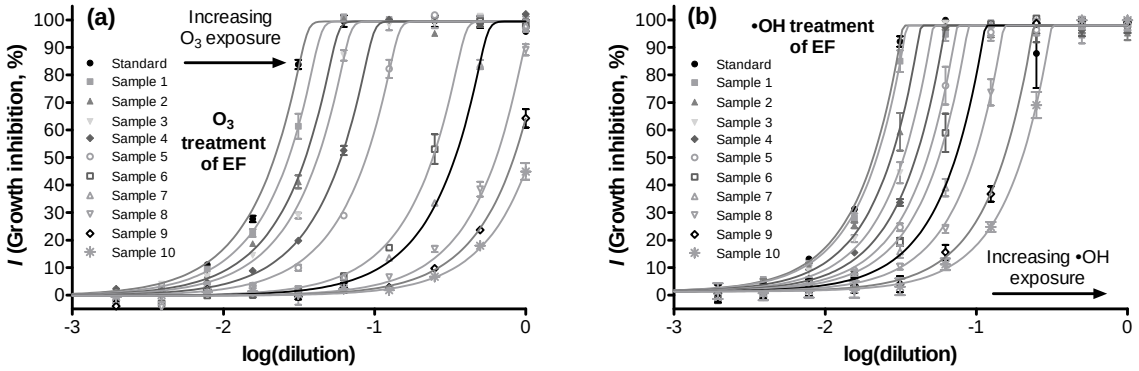

Figure S5. Dose-response relationships for oxidation of EF by (a) O_3 and (b) •OH. Measurements of *I* (symbols) are depicted with 95% confidence intervals determined for triplicate data sets, according to Text S3. Fits (lines) obtained using eq S2. The independent variable "dilution" is determined as described in the caption to Figure 1 in the main text.

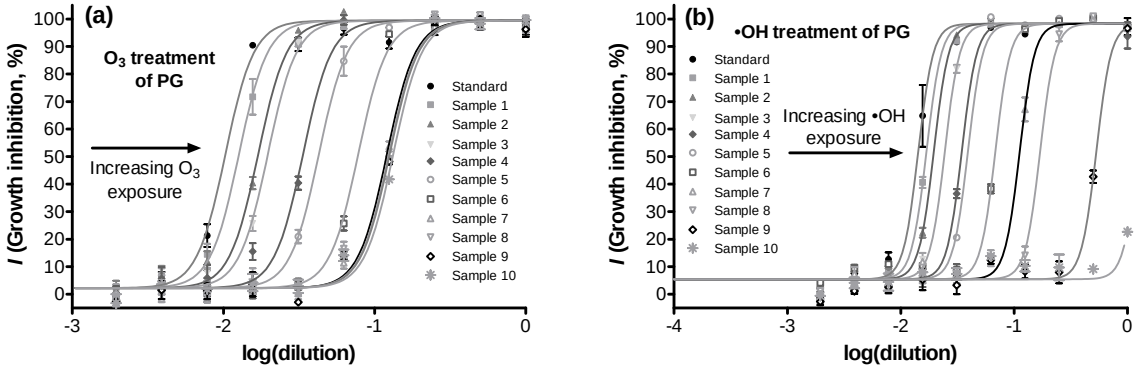

Figure S6. Dose-response relationships for oxidation of PG by (a) O_3 and (b) •OH. Measurements of *I* (symbols) are depicted with 95% confidence intervals determined for triplicate data sets, according to Text S3. Fits (lines) obtained using eq S1. The independent variable "dilution" is determined as described in the caption to Figure 1 in the main text.

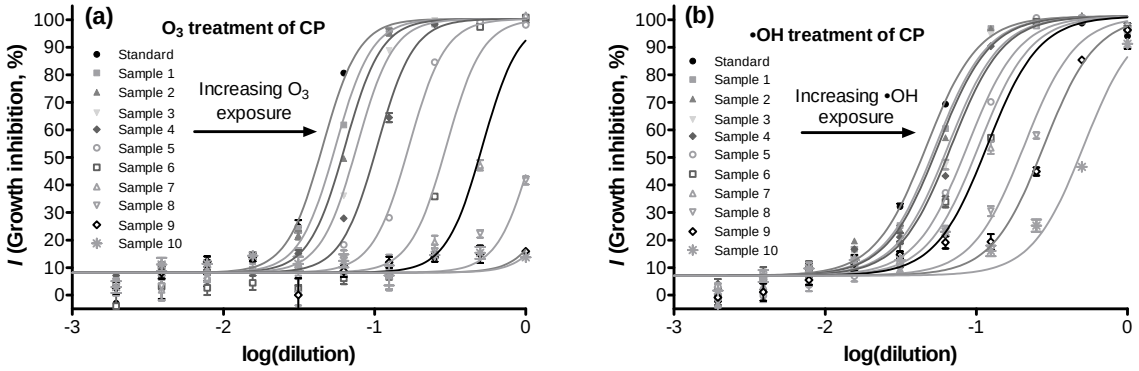

364

365 **Figure S7**. Dose-response relationships for oxidation of CP by (a) O_3 and (b) •OH.
366 Measurements of *I* (symbols) are depicted with 95% confidence intervals determined for
367 triplicate data sets, according to Text S3. Fits (lines) obtained using eq S1. The independent
368 variable "dilution" is determined as described in the caption to Figure 1 in the main text.

369

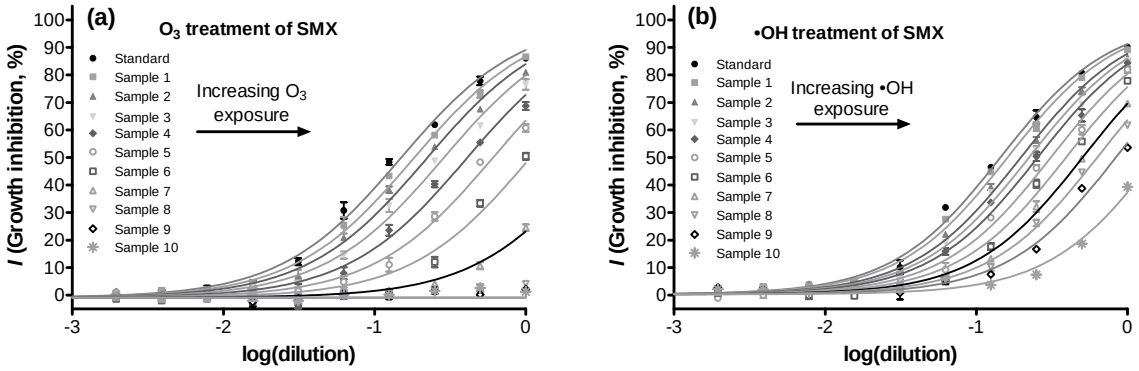

370

371 **Figure S8**. Dose-response relationships for oxidation of SMX by (a) O_3 and (b) •OH.
372 Measurements of *I* (symbols) are depicted with 95% confidence intervals determined for
373 triplicate data sets, according to Text S3. Fits (lines) obtained using eq S1. The independent
374 variable "dilution" is determined as described in the caption to Figure 1 in the main text.

375

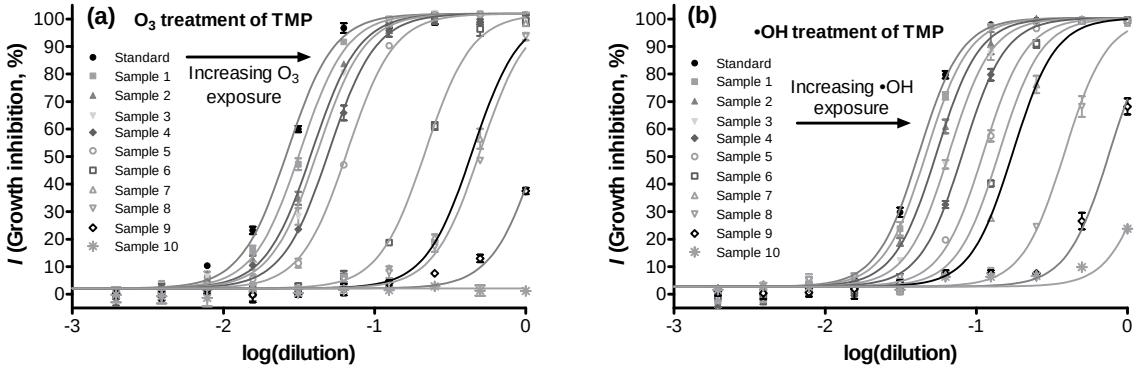

376

377 **Figure S9**. Dose-response relationships for oxidation of TMP by (a) O_3 and (b) •OH.
378 Measurements of *I* (symbols) are depicted with 95% confidence intervals determined for
379 triplicate data sets, according to Text S3. Fits (lines) obtained using eq S1. The independent
380 variable "dilution" is determined as described in the caption to Figure 1 in the main text.

381

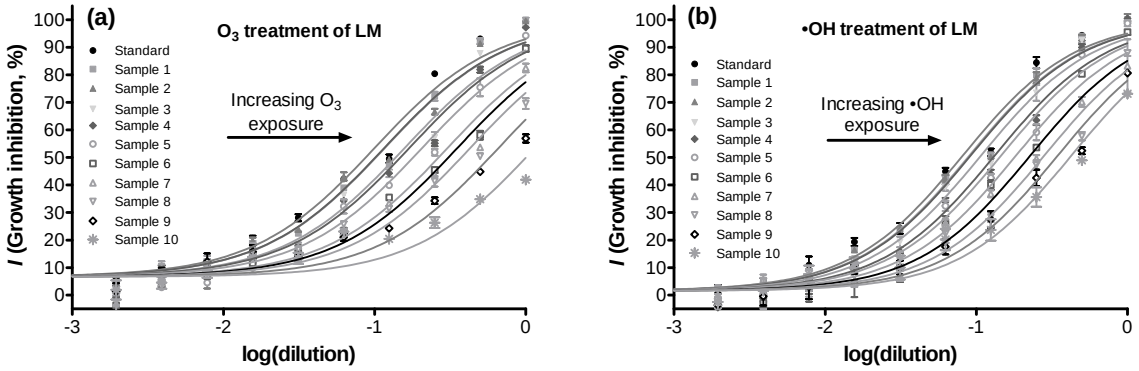

Figure S10. Dose-response relationships for oxidation of LM by (a) O_3 and (b) •OH. Measurements of *I* (symbols) are depicted with 95% confidence intervals determined for triplicate data sets, according to Text S3. Fits (lines) obtained using eq S1. The independent variable "dilution" is determined as described in the caption to Figure 1 in the main text.

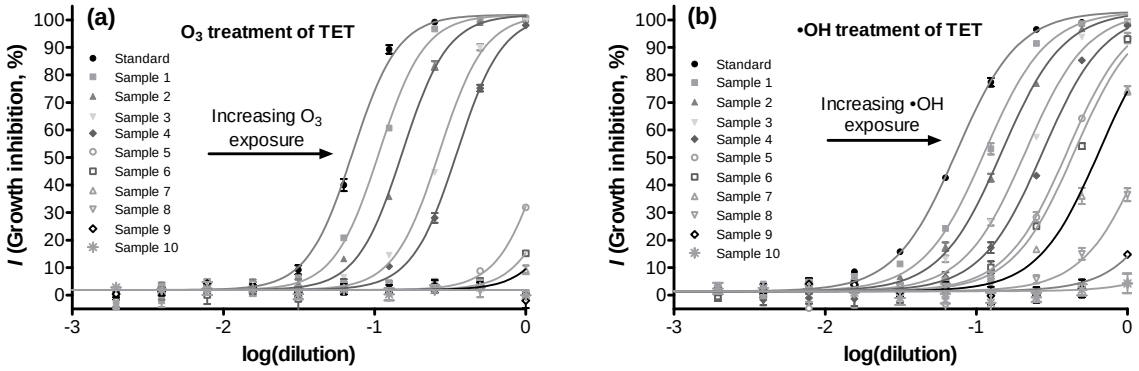

Figure S11. Dose-response relationships for oxidation of TET by (a) O_3 and (b) •OH. Measurements of *I* (symbols) are depicted with 95% confidence intervals determined for triplicate data sets, according to Text S3. Fits (lines) obtained using eq S1. The independent variable "dilution" is determined as described in the caption to Figure 1 in the main text.

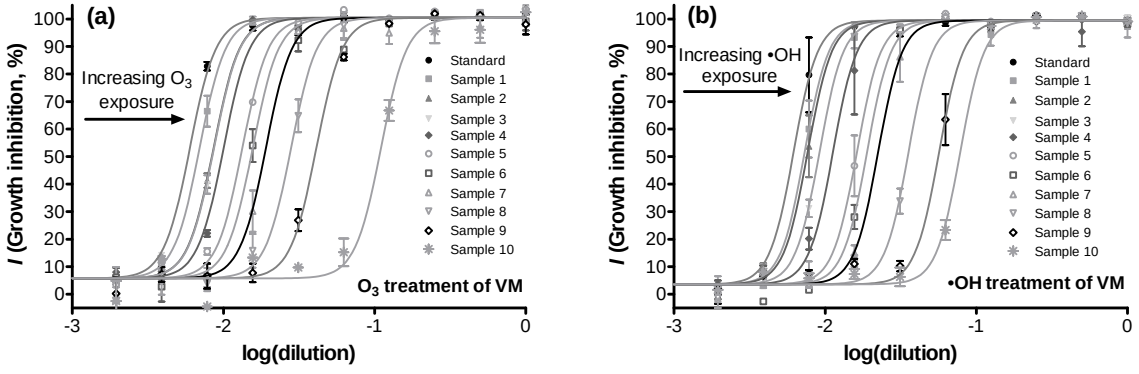

Figure S12. Dose-response relationships for oxidation of VM by (a) O_3 and (b) •OH. Measurements of *I* (symbols) are depicted with 95% confidence intervals determined for triplicate data sets, according to Text S3. Fits (lines) obtained using eq S1. The independent variable "dilution" is determined as described in the caption to Figure 1 in the main text.

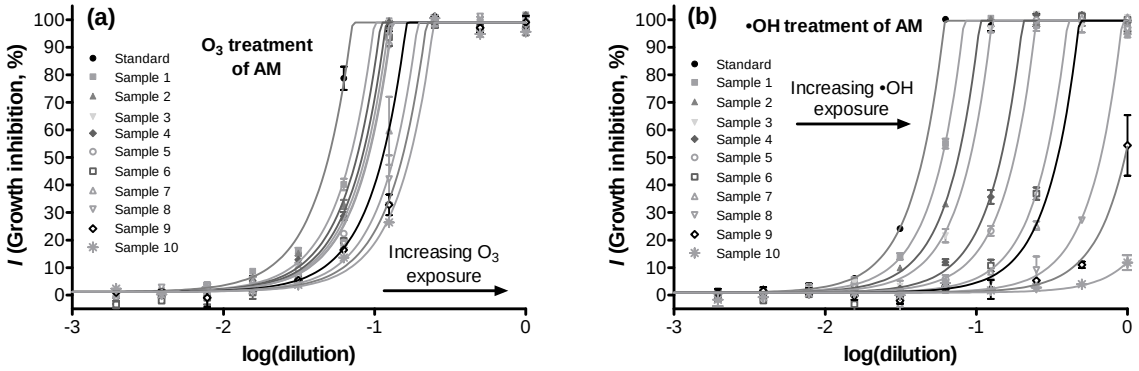

Figure S13. Dose-response relationships for oxidation of AM by (a) O_3 and (b) •OH. Measurements of *I* (symbols) are depicted with 95% confidence intervals determined for triplicate data sets, according to Text S3. Fits (lines) obtained using eq S2. The independent variable "dilution" is determined as described in the caption to Figure 1 in the main text.

Literature Cited

(1) Suarez, S.; Dodd, M. C.; Omil, F.; von Gunten, U. Kinetics of triclosan oxidation by aqueous ozone and consequent loss of antibacterial activity: Relevance to municipal wastewater ozonation. *Water Res.* **2007,** *41* (12), 2481-2490.

(2) Dodd, M. C.; Buffle, M.-O.; von Gunten, U. Oxidation of antibacterial molecules by aqueous ozone: Moiety-specific reaction kinetics and application to ozone-based wastewater treatment. *Environ. Sci. Technol.* **2006,** *40* (6), 1969-1977.

(3) Stead, D. A.; Richards, R. M. E. Sensitive fluorimetric detection of gentamicin sulfate in biological matrices using solid-phase extraction, pre-column derivatization with 9-fluoroenylmethyl chloroformate and reversed phase high-performance liquid chromatography. *J. Chromatogr. B* **1996,** *675*, 295-302.

(4) von Gunten, U.; Oliveras, Y. Advanced oxidation of bromide-containing waters: Bromate formation mechanisms. *Environ. Sci. Technol.* **1998,** *32* (1), 63-70.

(5) National Committee on Clinical Laboratory Standards. *Methods for Dilution Antimicrobial Susceptibility Tests for Bacteria that Grow Aerobically - Fourth Edition; Approved Standard*; NCCLS: Wayne, PA, 1997.

(6) Van der Graaf, P. H.; Schoemaker, R. C. Analysis of asymmetry of agonist concentration-effect curves. *J. Pharmacol. Toxicol. Methods* **1999,** *41* (2-3), 107-115.

(7) Lange, F.; Cornelissen, S.; Kubac, D.; Sein, M. M.; von Sonntag, J.; Hannich, C. B.; Golloch, A.; Heipieper, H. J.; Moder, M.; von Sonntag, C. Degradation of macrolide antibiotics by ozone: A mechanistic case study with clarithromycin. *Chemosphere* **2006,** *65* (1), 17-23.

(8) Walsh, C. *Antibiotics: Actions, Origins, Resistance*; ASM Press: Washington, D.C., 2003.

(9) Huber, M. M.; Canonica, S.; Park, G. Y.; von Gunten, U. Oxidation of pharmaceuticals during ozonation and advanced oxidation processes. *Environ. Sci. Technol.* **2003,** *37* (5), 1016-1024.

(10) Muñoz, F.; von Sonntag, C. The reactions of ozone with tertiary amines including the complexing agents nitrilotriacetic acid (NTA) and ethylenediaminetetraacetic acid (EDTA) in aqueous solution. *J. Chem. Soc. Perk. Trans. 2* **2000,** (10), 2029-2033.

(11) Shen, L. L.; Mitscher, L. A.; Sharma, P. N.; O'Donnell, T. J.; Chu, D. W. T.; Cooper, C. S.; Rosen, T.; Pernet, A. G. Mechanism of inhibition of DNA gyrase by quinolone antibacterials: a cooperative drug-DNA binding model. *Biochemistry-US* **1989,** *28* (9), 3886-3894.

(12) Chan, W. F.; Larson, R. A. Formation of mutagens from the aqueous reactions of ozone and anilines. *Water Res.* **1991,** *25* (12), 1529-1538.

(13) Mvula, E.; von Sonntag, C. Ozonolysis of phenols in aqueous solution. *Org. Biomol. Chem.* **2003,** *1* (10), 1749-1756.

(14) Matsui, M.; Shibata, K.; Muramatsu, H.; Nakazumi, H. Ozonolyses of cytosines and guanine. *J. Org. Chem.* **1991,** *56* (16), 4987-4990.

(15) Flyunt, R.; Theruvathu, J. A.; Leitzke, A.; von Sonntag, C. The reactions of thymine and thymidine with ozone. *J. Chem. Soc., Perkin Trans. 2* **2002,** (9), 1572-1582.

(16) Matthews, D. A.; Bolin, J. T.; Burridge, J. M.; Filman, D. J.; Volz, K. W.; Kaufman, B. T.; Beddell, C. R.; Champness, J. N.; Stammers, D. K.; Kraut, J. Refined crystal

structures of *Escherichia coli* and chicken liver dihydrofolate reductase containing bound trimethoprim. *J. Biol. Chem.* **1985,** *260* (1), 381-391.

(17) Qiang, Z.; Adams, C.; Surampalli, R. Determination of ozonation rate constants for lincomycin and spectinomycin. *Ozone Sci. Eng.* **2004,** *26* (6), 525-537.

(18) Spry, D. O. Oxidation of penicillin and dihydrocephalosporin derivatives with ozone. *J. Org. Chem.* **1972,** *37* (5), 793-795.

(19) Bailey, P. S. *Ozonation in organic chemistry. II. Non-olefinic compounds*; Academic Press: New York, NY, 1982.

(20) Sztaricskai, F.; Dinya, Z.; Batta, G.; Mocsári, A. Chemical synthesis and structural study of lincomycin sulfoxides and a sulfone. *J. Antibiot.* **1997,** *50* (10), 866-873.

(21) Schlünzen, F.; Zarivach, R.; Harms, J.; Bashan, A.; Tocilj, A.; Albrecht, R.; Yonath, A.; Franceschi, F. Structural basis for the interaction of antibiotics with the peptidyl transferase centre in eubacteria. *Nature* **2001,** *413*, 814-821.

(22) Dowideit, P.; von Sonntag, C. Reaction of ozone with ethene and its methyl- and chlorine-substituted derivatives in aqueous solution. *Environ. Sci. Technol.* **1998,** *32* (8), 1112-1119.

(23) Chopra, I.; Roberts, M. Tetracycline antibiotics: Mode of action, applications, molecular biology, and epidemiology of bacterial resistance. *Microbiol. Mol. Biol. Rev.* **2001,** *65* (2), 232-260.

(24) Ragnar, M.; Eriksson, T.; Reitberger, T.; Brandt, P. A new mechanism in the ozone reaction with lignin like structures. *Holzforschung* **1999,** *53* (4), 423-428.

(25) Kadurugamuwa, J. L.; Lam, J. S.; Beveridge, T. J. Interaction of gentamicin with the A band and B band lipopolysaccharides of *Pseudomonas aeruginosa* and its possible lethal effect. *Antimicrob. Agents Chemother.* **1993,** *37* (4), 715-721.

(26) Dodd, M. C.; Rentsch, D.; Singer, H. P.; Kohler, H.-P. E.; von Gunten, U. Transformation of β-lactam antibacterials during aqueous ozonation: Reaction mechanisms and quantitative bioassay-directed characterization of biologically-active oxidation products. *In preparation*.